Astron. Astrophys. 318, 621–630 (1997)

ASTRONOMY
AND
ASTROPHYSICS

The form of ideal current layers and kink instability in line-tied coronal loops

H. Baty

Observatoire Astronomique, 11 Rue de l'Université, F-67000 Strasbourg, France

Received 28 March 1996 / Accepted 3 July 1996

Abstract. We have investigated the characteristics of the current concentration which develops when an unstable line-tied coronal loop is driven by an ideal kink instability towards a secondary bifurcated magnetohydrodynamic (MHD) equilibrium. Using fully three dimensional MHD simulations in cylindrical geometry, the main results indicate an algebraic linear-like dependence of the thickness and amplitude of the current concentration on the aspect ratio of the loop. A simple model is proposed, which interprets this scaling in terms of the axial field line bending effect due to the line-tying constraints in the kinked configuration. Indeed, a curvature force term arises and prevents the formation of a current sheet, which is known to develop in un-tied configuration. For the typical parameters of observed loops, the thickness of the current layer is approximately two or three orders of magnitude smaller than the length scale of the initial equilibrium. Finally, we discuss the subsequent current dissipation and the efficiency with which such a mechanism can heat the corona.

Key words: sun: corona – MHD – methods: numerical – instabilities

1. Introduction

The heating of the solar corona is an important problem of solar physics. It remains unsolved despite considerable efforts to propose efficient heating mechanisms. It is commonly admitted that the basic source of free energy is the photospheric plasma flow associated with convection. However, depending on the way this mechanical energy is supplied to the corona, the heating theories can be classified as either wave or current dissipation theories.

Wave heating is based on the generation of Alfvèn waves by the photospheric motions with a time scale of the order of the Alfvèn transit time scale. These waves propagate and may be subsequently dissipated within the corona by either phase-mixing (Heyvaerts & Priest 1983) or resonant absorption (Ionson 1978; Hollweg 1987; Einaudi & Mok 1987). Although the dissipation coefficients are extremely small, wave dissipation can be an efficient mechanism because large gradients develop during these processes. Presently, the wave heating theory is under intense investigation (Halberstadt & Goedbloed 1993–1995; Califano et al. 1992).

Although the heating by Alfvèn waves is a viable mechanism for open magnetic field region (coronal holes) and quiet closed field region, electric current dissipation mechanisms including magnetic reconnection are likely to dominate in active regions.

In current dissipation theory, the continuous twisting or braiding of magnetic flux tubes by photospheric motions on a slow time scale (compared with the Alfvèn transit time) is considered. This can drive fine scale current systems and subsequently rapid energy dissipation (Heyvaerts 1992). Parker (1983) proposed that the coronal magnetic structure becomes increasingly more complex due to braiding of magnetic field lines by complex photospheric boundary motions, and finally reaches an highly dissipative state. An approximate statistical description of the effect of magnetic braiding on the coronal electric system has been developed by Van Ballegooijen (1986). He has shown that the electric current develops a spectrum that reaches finer and finer scales as time goes on. Other authors, following Chiuderi (1980), have argued that a gradient length short enough for dissipation could result from MHD resistive instabilities developing in stressed coronal magnetic structures. Heyvaerts and Priest (1984, 1992), considering that initial instabilities should develop into a turbulent regime that would lead to dissipation, have presented global descriptions for coronal heating produced by a turbulent solar corona.

This paper deals with a particular aspect of these problems, namely, the development of the kink instability in line-tied coronal loops. The ideal MHD kink instability is one of the routes by which fine-scale current structures may form in the solar coronal medium. Although the dissipation coefficients are extremely small, dissipative effects would then rapidly destroy the almost singular current layers or filaments that are expected to form as a result of this instability, eventually leading to heating of the medium. In a recent paper, Longcope et al. (1994) have shown that (genuine) current sheets cannot develop in the ideal evolution of the line-tied coalescence instability. This result is

consistent with recent numerical results of an MHD simulation on the ideal kink instability in line-tied cylindrical loop by Baty & Heyvaerts (1996). Therefore, more work remains to be done to describe in detail the mechanism by which kink instabilities could produce extremely fine-scale current gradients in line-tied cylindrical loops.

Coronal loops are magnetic flux tubes anchored in the photosphere. Because of the large density and small resistivity of the photospheric fluid, the magnetic field lines can be considered as "frozen" in the photospheric flow, which twists magnetic flux tube, i.e. induces currents in them, injecting magnetic energy into the loops. However, magnetic energy storage cannot proceed further if the loop becomes unstable on a time scale that is shorter than that of photospheric motions. Cylindrical line tied loops have been found to be ideally unstable when a critical twist is exceeded (Raadu 1972; Hood & Priest 1979; Einaudi & Van Hoven 1983). The twist is the change of the azimutal angle of a point following a given field line from one photospheric boundary to the other. Long and thin coronal loops are considered, so that, to a first approximation, toroidal curvature effects can be neglected in this study. The critical twist value depends on the aspect ratio and on the equilibrium configuration, the aspect ratio being the ratio of the loop length to its radius. The linear structure of the kink is fairly well established (Velli et al. 1990a; Mikic et al. 1990; Baty & Heyvaerts 1996). Although its structure bears some resemblance with the internal kink mode in cylindrical periodic geometry (representative of magnetic confinement devices for nuclear fusion, such as tokamaks and pinchs), the line-tying conditions suppress resonant singular surfaces. In addition, the mode has a ballooning character with a maximum amplitude at the axial midplane. However, few results are available on the non linear evolution of the mode. Strauss & Otani (1988) have performed numerical calculations in cylindrical geometry using a set of reduced MHD equations. Current sheets have been shown to form as in the periodic case, but no discussion of the circumstances under which this happens has been presented, and a non-zero resistivity was included to smooth the solution. Craig & Sneyd (1990) have also addressed this issue, using incompressible Lagrangian numerical calculations for the uniform twist Gold-Hoyle cylindrical line-tied flux tube; and they found that current sheets mainly appear near the tube ends. Finally, no current sheets formed in the line-tied cases treated by Mikic et al. (1990), because the loop was too short. In a recent paper, we clarified the situation by highlighting the mechanism by which fine-scale current structures may form (Baty & Heyvaerts 1996). Using fully three dimensional non linear MHD simulations in line-tied cylindrical loops, we considered two distinct initially unstable equilibria, the uniform-twist force-free Gold-Hoyle profile (GH) and a non force-free field with variable and localized twist profile (LT). For these two equilibria, the initial magnetic equilibrium has been shown to reach a bifurcated ideal MHD equilibrium. For the GH case, the magnetic structure obtained exhibits only non linear deformation of the initial equilibrium without formation of a fine scale magnetic structure. This results from the somewhat "pathological" character of the GH equilibrium, the twist of which having a constant value as a function of the radius (i.e. there is no shear). However, a current concentration extending all along the loop length and taking the form of an helical ribbon of intense current has been obtained for the LT case. This current concentration is non singular in the sense that it appears as a negative current spike with finite amplitude and non zero thickness. This contrasts with periodic configurations where a singular current sheet forms in the ideal limit. In the case of the loop studied by Baty & Heyvaerts, the thickness of the current layer has been found to be two orders of magnitude smaller than the loop radius. As pointed out by Mikic et al. (1990), the length of the loop probably plays an important role in determining the characteristics of the current layer. Line-tying effects should become less important for longer loop lengths, and a singular current sheet should form in the limit of infinite length. Recently, similar current concentrations have been obtained during the development of the sausage instability in coronal loops (Longbottom et al. 1996).

The aim of this paper is to investigate the dependence on the initial equilibrium parameters of the characteristics of the ideal current layer generated by the kink instability in line-tied solar loops. It is of particular interest to study how the thickness and the amplitude of the current concentration scales with the aspect ratio of the loop. We assume resistive effects to become important only in the non linear development, when the ideal kink mode has brought the initial equilibrium to a bifurcated kinked configuration. We plan to study the effect of resistivity in a future work. We do not deal here with resistive kink or tearing modes (Velli et al. 1990b; Otani & Strauss 1988; Mok & Van Hoven 1982) for which resistivity has an important effect on stability limits and on the dynamics of the linear phases. Numerical computations of ideally unstable kink modes have been carried out using the full 3D cylindrical non linear evolution MHD code, SCYL (Baty & Heyvaerts, 1996).

This paper is organised as follows. The physical model is presented in Sect. 2, where the numerical procedure is also briefly described. In Sect. 3, we present the initial unstable equilibria used as starting point of the simulations, and we give a brief study of the stability and of the linear phase of the kink mode. Results on the non linear development of the kink instability are reported in Sect. 4. A simple model is also provided to interpret the scaling of the characteristics of the current layer with the aspect ratio of the loop. Finally, in Sect. 5, we discuss the results with a particular attention on the consequences on the heating of the medium.

2. Physical model

As pointed out in Sect. 1, we restrict our attention to the usual cylindrical geometry approximation. As seen in Fig. 1, the solar loop is modelled by a flux tube of length L, with foot points of magnetic field lines anchored in the photosphere, at two end-plates at $z = \pm L/2$. To start the numerical simulation, we have used magnetic equilibria twisted locally by the photospheric flow. Adding an arbitrary small $m = 1$ perturbation (m being the azimuthal mode number), we followed the dynamic evolution

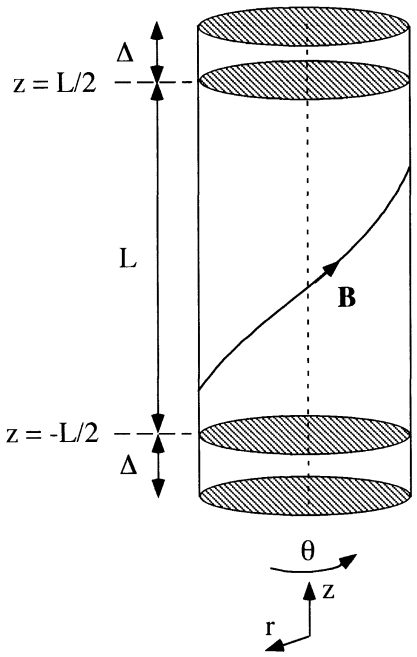

Fig. 1. Cylindrical model of the twisted flux tubes. The corona extends beween $z = L/2$ and $z = -L/2$, and the photosphere has an axial extent Δ

of the system on a fast time scale as compared with the slow photospheric time scale. The coronal perturbations are forced to vanish at the ends of the loop because of the inertial anchoring that gives rise to the line-tying conditions. We impose all the components of the perturbations vanish at the photosphere, i.e. we use the usual rigid plates conditions (Velli et al. 1990a). The photosphere is supposed to have a finite axial extent Δ, to simplify the numerical approach. More details about the effects of the numerical extent of the photospheric part are given by Baty & Heyvaerts (1996), who found that the results are not sensitive to the exact value of Δ as long as it remains large enough compared to the smallest axial scale length included in the simulation.

An arbitrary radial boundary condition is also assumed, which is a perfectly conducting wall placed at $r = a$ in order to simplify the computation. The position of this wall will produce negligible effects provided the wall is far enough away from the loop axis (Hood & Priest 1981; Craig et al. 1988; Mikic et al. 1990).

2.1. Equations

Numerical computations are carried out using our code, SCYL, which solves the following full set of compressible and dissipative MHD equations, which can be written as (in non dimensional form):

$$\frac{\partial \rho}{\partial t} + \nabla \cdot (\rho \boldsymbol{v}) = 0\,, \tag{1}$$

$$\rho \left[\frac{\partial \boldsymbol{v}}{\partial t} + \boldsymbol{v} \cdot \nabla \boldsymbol{v} \right] = \boldsymbol{J} \times \boldsymbol{B} - \nabla P + \mu \nabla^2 \boldsymbol{v}\,, \tag{2}$$

$$\frac{\partial P}{\partial t} + \boldsymbol{v} \cdot \nabla P = -\gamma P \nabla \cdot \boldsymbol{v}\,, \tag{3}$$

$$\frac{\partial \boldsymbol{B}}{\partial t} = \nabla \times (\boldsymbol{v} \times \boldsymbol{B}) - \nabla \times (\eta \boldsymbol{J})\,, \tag{4}$$

$$\boldsymbol{J} = \nabla \times \boldsymbol{B}\,. \tag{5}$$

Here, ρ is the mass density, P the plasma pressure, $\boldsymbol{v}$ the fluid velocity, $\boldsymbol{B}$ the magnetic field, $\boldsymbol{J}$ the electric current density. η and μ are the magnetic diffusivity and the kinematic viscosity respectively, and γ is the ratio of specific heats (a value of 5/3 is used). The Lundquist number S, which is the ratio of the diffusion time t_r to the Alfvén time t_a, is $S = 1/\eta(0)$, $\eta(0)$ being the value of the resistivity on the magnetic axis. The energy equation is as simplified as possible, describing only energy convection (Eq. (3)) because the aim of the simulation is primarily to understand the dynamics. It would be easy to modify Eq. (3) to include thermal conductivity, and we plan to do so in future work.

The variables are normalized as follows:

$$\rho \rightarrow \frac{\rho}{\rho_0}, t \rightarrow \frac{t}{t_\mathrm{a}}, \boldsymbol{r} \rightarrow \frac{\boldsymbol{r}}{a}, \boldsymbol{B} \rightarrow \frac{\boldsymbol{B}}{\boldsymbol{B}^*}, \boldsymbol{v} \rightarrow \frac{\boldsymbol{v}}{v_\mathrm{a}}, P \rightarrow \frac{P}{(B^{*2}/\mu_0}\,, \tag{6}$$

$$\text{with } v_\mathrm{a}^2 = \frac{B^{*2}}{\rho_0 \mu_0},\ t_\mathrm{a} = \frac{a}{v_\mathrm{a}},\ t_\mathrm{r} = \frac{\mu_0 a^2}{\eta},\ t_\mathrm{v} = \frac{\rho_0 a^2}{\mu},\ S = \frac{t_\mathrm{r}}{t_\mathrm{a}}\,, \tag{7}$$

where a is the radius of the flux tube, ρ_0 the density at the radial boundary $r = a$ and B^* a reference magnetic field value given by $B^* = B(0) 2\pi a / L_\mathrm{t}$ ($B(0)$ being the magnetic field value on the axis and L_t the full length of the cylinder, $L_\mathrm{t} = L + 2\Delta$).

Again, we discuss only ideal MHD dynamics (i. e. $\eta = 0$).

2.2. The numerical procedure

The MHD equations (1–5) are integrated in time with an efficient semi-implicit method allowing large time steps, limited by the non linear physical plasma phenomena, and ensuring a high spatial resolution (Lerbinger & Luciani 1991). The scheme is linearly fully implicit, and the stability is ensured by adding a small elliptic operator in the non linear phases. This elliptic operator dominates only the non linear magnetic perturbation, and is much smaller in size than elliptic operators usually used in semi-implicit methods where it has to dominate the equilibrium magnetic field contribution to ensure numerical stability. The diffusive terms are treated fully implicitly, and a second order predictor-corrector scheme has been developed applying the semi-implicit operator both at the predictor and corrector levels.

The periodic version of the code, XTOR, has been used previously to study the non linear magnetic reconnection process associated with the $m = 1$ internal kink instability in tokamak, in cylindrical geometry (Baty et al. 1991) and in toroidal geometry (Baty et al. 1992, 1993). The line-tied cylindrical version, XCYL, has proved its ability to simulate long time MHD evolution together with a high spatial resolution in a line-tied solar context (Baty & Heyvaerts 1996).

Cylindrical coordinates (r,Θ,z) are used, with r the radial coordinate (labelling equilibrium magnetic surfaces), Θ the azimuthal angle, and z the axial coordinate. Radially, we use finite

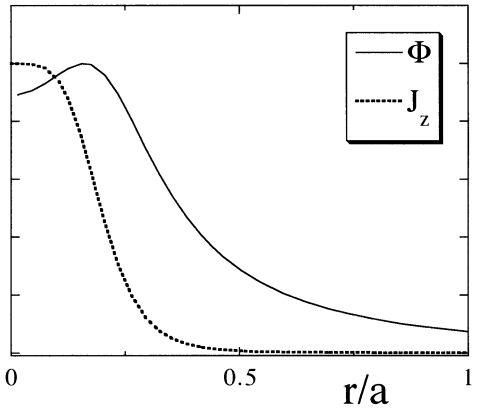

Fig. 2. The twist Φ profile as a function of the normalized radius r/a (in arbitrary units), and J_z the resulting axial component of the current density

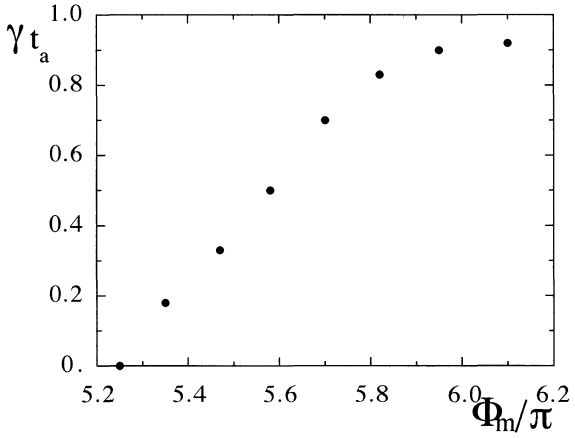

Fig. 3. The linear $m = 1$ growth rate γ for an aspect ratio value $L/a = 4.7$, as a function of the twist

differences on two staggered meshes. Variables are expanded in double Fourier series in Θ and ϕ ($\phi = z2\pi/L_t$) and operations are performed using a fast Fourier transform (FFT). We use 100 grid points in the radial direction with the possibility of accumulation in the vicinity of current layers. For the other directions, $24 * 128$ grid points are used in $\Theta * z$.

In order to get a precise description of the modes, we adopt a "de-aliasing" procedure in the axial direction as well as in the Θ direction. Indeed, when FFT's are used, "aliasing" errors introduced by the discrete transforms quickly degrade the solution, especially in the higher harmonics (Aydemir & Barnes 1985). In this work, we use up to 7 modes, each with a band of 80 axial harmonics centered around the fastest growing axial harmonic (Einaudi & Van Hoven 1983).

At the outer perfectly conducting boundary wall at $r = a$, we imposed a vanishing radial component of the velocity together with the usual electromagnetic boundary conditions on the electric and magnetic fields.

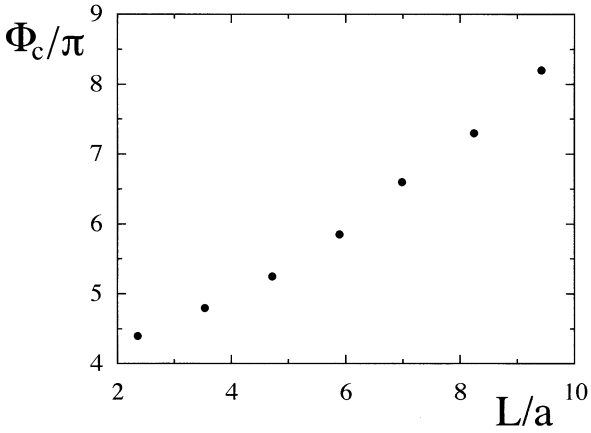

Fig. 4. The critical twist value Φ_c as a function of the aspect ratio L/a

3. Equilibrium, stability, and linear phase

3.1. Equilibrium

Mikic et al. (1990) have calculated the equilibrium magnetic configuration which result from an imposed localized photospheric flow. Such equilibria are two dimensional with radial and axial dependences. However, it is apparent from their results (see Fig. 4) that the equilibrium quantities are independent of the axial coordinate z over most of the loop length except in narrow boundary layers near the photosphere. Neglecting the z dependence of the initial equilibrium, Baty & Heyvaerts (1996) have shown that the effects on the stability are negligible. Therefore, for the sake of simplification, we consider one dimensional (radial) force-free equilibria. Such equilibria are fully determined by the radial profile of a function which can be taken to be the magnetic twist angle Φ. For a flux tube of length L, the twist angle measured from $z = -L/2$ to $z = L/2$ is given by the following expression:

$$\Phi(r) = \frac{LB_\Theta}{rB_z}\,, \tag{8}$$

with B_Θ and B_z the azimuthal and axial components of the equilibrium magnetic field. In this study, we adopt localized twist profile as shown in Fig. 2. The resulting axial profile of the current density is also plotted in Fig. 2. The current density appears to be mainly confined within $r = 0.5a$.

3.2. Stability

For a given loop length, the equilibrium is kink unstable when the twist exceeds a critical value Φ_c (Hood & Priest 1979; Einaudi & Van Hoven 1983; Mikic et al. 1990; Velli et al. 1990; Baty & Heyvaerts 1996). Indeed, in Fig. 3, we have plotted the linear growth rate of the ideal $m = 1$ kink mode as a function of the twist angle Φ_m, for an aspect ratio $L/a = 4.7$. Φ_m is the maximum twist value, obtained near $r = 0.15a$, as can be seen in Fig. 2. Each point has been obtained for a vanishing viscosity (a dissipation time $t_v = 10^6\, t_a$ is used), and after optimization of Δt the time step and Δr the radial grid resolution. Then, we

have investigated the dependence of the critical twist value as a function of the aspect ratio of the loop. The results are plotted in Fig. 4, showing a good agreement with the typical dependence found by Hood & Priest (1979).

3.3. Linear properties of the kink mode

The linear structure of the kink mode can be said to be fairly well established (Mikic et al. 1990; Velli et al. 1990; Baty & Heyvaerts 1996). At the axial midplane of the loop, the mode takes the form of a cellular convection pattern with a continuous radial displacement. As far as the axial structure is concerned, the mode amplitude vanishes at the photosphere and balloons out with a maximum value at the axial midplane. Contrary to periodic geometry (Rosenbluth et al. 1973), resonant magnetic surfaces are absent due to the line tying effect. As a consequence singular layers are suppressed. The only "resonant point" is a point located at the axial midplane of the loop where the radial component of the perturbed magnetic field vanishes, and corresponds to a resonance condition $\boldsymbol{k} \bullet \boldsymbol{B} = 0$ ($\boldsymbol{k}$ being the local wave vector of the mode and $\boldsymbol{B}$ the equilibrium magnetic field). It has been shown that this point coincides with the location where the current concentration develops during the further evolution of the configuration (Baty & Heyvaerts 1996).

4. The non linear development of the kink instability

The initial magnetic equilibrium is expected to be driven towards a secondary bifurcated MHD equilibrium by the ideal kink (Baty & Heyvaerts 1996). Therefore, we have used a numerical procedure where viscous dissipation has been progressively added to rapidly find this kinked equilibrium, avoiding numerical oscillations. Typically, this artificial dissipation time was $t_{\rm v} = 10^5\, t_{\rm a}$ at the beginning of the simulation, and $t_{\rm v} = 10^2\, t_{\rm a}$ at the end. We have selected 7 unstable magnetic equilibrium configurations corresponding to aspect ratios between 2 and 10. In order to simplify the interpretation of the results, we have chosen the value of the twist in order to have cases with linear growth rates of order $0.4\, t_{\rm a}^{-1}$.

4.1. Simulation results

Our results show the development of a current concentration during the non linear development of the kink instability. At the axial midplane of the loop, this current concentration is localized at the "resonant point" described above. And, it extends all along the loop, in the form of an helical ribbon of intense current. Its radial location and its amplitude exhibit an axial modulation along the loop because of the line-tying effect. The typical structure of the axial component of the current density can be seen in Fig. 5.

The secondary bifurcated equilibrium is considered to be reached when the flow associated with the instability is fully dissipated by viscosity, and when the displacement of the magnetic axis has stopped. A typical time evolution (for the case $L/a = 4.7$) of the radial location of the magnetic axis as a function of time is plotted in Fig. 6. In this Figure, by comparing the values for $z = 0$ and $z = L/4$, one should also note the axial modulation of the displacement.

We have measured the maximum amplitude of the current concentration $J_{\rm m}$, which is reached at the axial midplane of the loops for the bifurcated equilibria. The results are plotted as a function of the aspect ratio in Fig. 7, showing an increasing linear-like dependence. We have also measured the radial thickness of the current layer, which appears to have a decreasing linear-like behaviour. We stress that it is necessary to have a good enough spatial resolution in the computations, in order to be able to distinguish between a genuine current sheet and an intense current layer of non-zero thickness. We have been able to do so by using a radial accumulation with a grid resolution Δr of order 10^{-3}. The complicated three dimensional current layer structure makes it difficult to measure its thickness for the other axial midplanes with $z \neq 0$. Fortunately, the amplitude of the current can be precisely measured, and typical axial variations are plotted in Fig. 8. Let us now turn to the interpretation of these results.

4.2. Interpretation

In a periodic geometry, the kink instability is linearly a $m = n = 1$ perturbation (n being the axial mode number) which is associated to a quasi-rigid shift of a central column. The non linear evolution of the ideal kink mode leads to a secondary kinked MHD equilibrium containing an helical singular current sheet located at the $\Phi = 2\pi$ magnetic surface. This singularity corresponds to a discontinuity in the magnetic field and appears as a negative current spike with a vanishing thickness (or equivalently an infinite amplitude) (Park et al. 1980; Rosenbluth et al. 1973). In particular, the kinked configuration is characterized by a discontinuity at the radius location $r_{\rm s}$ of the helical field component $B_{\rm h}$, which is defined as the projection of the magnetic field on the wave vector $\boldsymbol{k} = (1/r, -2\pi/L)$. Then, at the $\Phi = 2\pi$ magnetic surface, the lines of force have the same pitch as the $m = n = 1$ kink perturbation. A simplified version of this configuration in slab geometry is shown in Fig. 9 (a) and (b), replacing $r - r_{\rm s}$ by x and $B_{\rm h}$ by $B_{\rm y}$. When crossing the $\Phi = 2\pi$ surface, the helical field undergoes a jump, the other components of the magnetic field being approximately constant. Although this discontinuity induces a singularity in the current density, the equilibrium is achieved because the jump is antisymmetric (Waelbroeck 1989).

It has been seen that the essential difference between line-tied and periodic geometries is an axial modulation, sometimes called a ballooning effect since it bears some resemblance with ballooning instabilities in tokamaks. In Fig. 10, we have plotted typical projections of the field lines on the (r,z) plane, as obtained in our simulations for a kinked equilibrium. One can observe the curvature of the perturbed magnetic field, due to the line-tying effect. As the radial location of the current concentration is at $r = 0.42a$ in this case, the magnetic field appears to be mostly curved in the innermost part before the current layer,

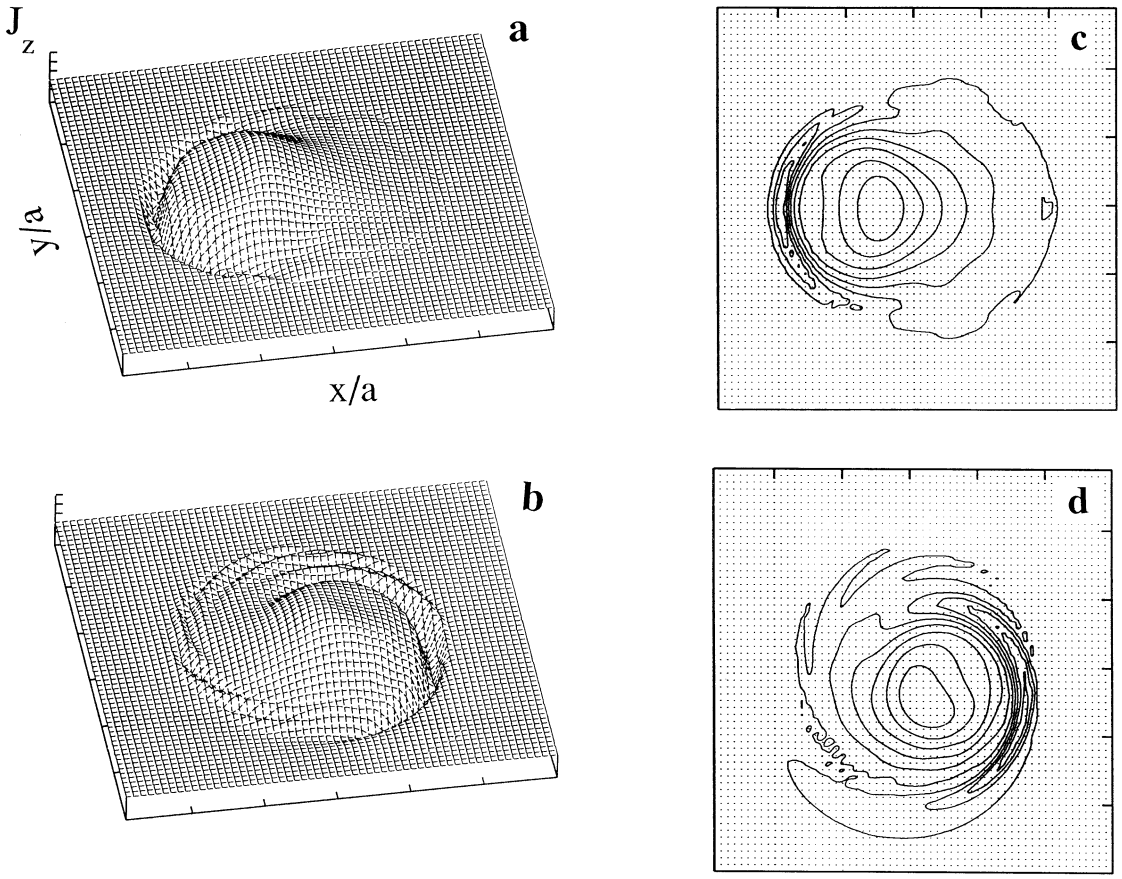

Fig. 5a–d. The axial component of the current density for the two axial planes: **a** $z = 0$ and **b** $z = L/4$, and the corresponding iso-contours: **c** for $z = 0$ and **d** for $z = L/4$

and the curvature radius varies with the field line considered (i.e. there is a "diffuse" curvature effect). Now, if one simply superposes this diffuse curvature effect to the simple model shown in Fig. 9, a line-tied model in slab geometry can be deduced as illustrated in Fig. 11a. In the vicinity of the current layer and near the axial midplane of the loop, this configuration would be in radial equilibrium if:

$$B_{\rm y}\frac{dB_{\rm y}}{dx} + B_{\rm z}\frac{dB_{\rm x}}{dz} = 0\,. \tag{9}$$

The main effect is to prevent the formation of the discontinuity in the magnetic field component $B_{\rm y}$, and to lead to an equilibrium between gradients in $B_{\rm y}$ and curvature force in the vicinity of the layer essentially in a region between $x = -2e$ and $x = 0$. In order to characterize the configuration in more details, in the above described region, we assume a simple linear dependence with x of the magnetic field component $B_{\rm y}$:

$$B_{\rm y}(x) = A\,x\,, \tag{10}$$

with A to be determined later (see Fig. 11b). The magnetic field component $B_{\rm x}$ can be obtained from the field line equation:

$$\frac{dx}{dz} = \frac{B_{\rm x}}{B_{\rm z}}\,. \tag{11}$$

Then, replacing Eqs.(10) and (11) in Eq.(9), one obtains:

$$A^2 x + B_{\rm z}^2\frac{d^2x}{dz^2} = 0\,, \tag{12}$$

where $B_{\rm z}$ has been assumed constant in this region. The expression (12) can be re-written as:

$$A^2 x + \frac{B_{\rm z}^2}{R_{\rm c}} = 0\,, \tag{13}$$

with $R_{\rm c}$ the local curvature radius defined by:

$$R_{\rm c} = \left[\frac{d^2x}{dz^2}\right]^{-1}\,, \tag{14}$$

which depends on the field line considered (see Fig. 10). Now, applying the force balance given by Eq. (13) at the middle of the region (i. e. for $x = -e$), one obtains:

$$e = \frac{1}{A^2}\frac{B_{\rm z}^2}{R_{\rm c}}\,, \tag{15}$$

which gives an expression for the length scale of the current gradient. To facilitate comparison with the simulation results,

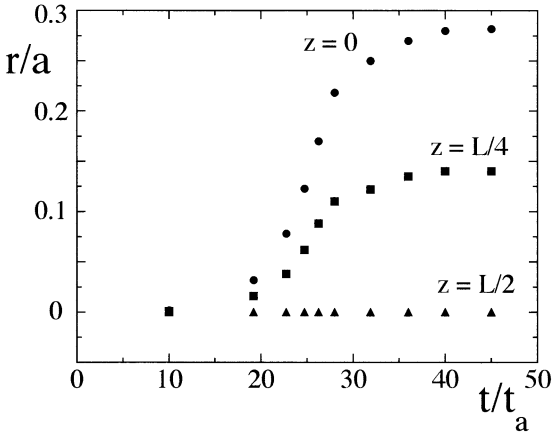

Fig. 6. The time evolution of the normalized radial location of the magnetic axis, for three axial planes $z = 0$, $z = L/4$, and $z = L/2$

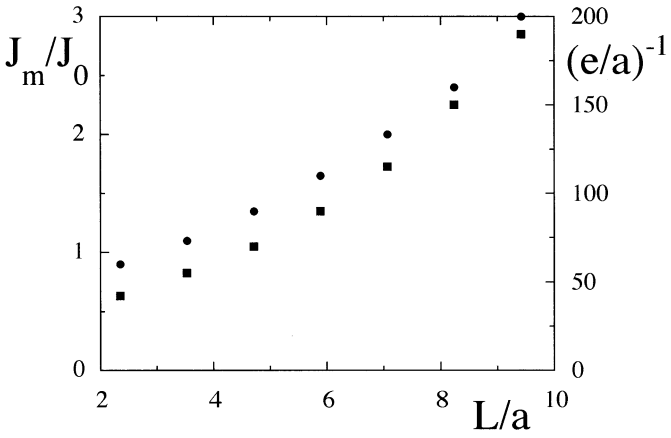

Fig. 7. The amplitude of the normalized current concentration (circles) and the normalized thickness of the current layer (squares) as a function of the aspect ratio L/a, measured at the axial midplane $z = 0$

we assume a simple sinusoidal form for the field lines in the x-z plane:

$$x = C\cos(\frac{\pi}{L}z) + x_0\,, \tag{16}$$

with x_0 a constant, which is the location of the field lines at the photosphere, and C an amplitude factor which depends on the field line considered. At the axial midplane of the loop ($z = 0$), the curvature radius can then be reduced to the following expression:

$$R_c = \left(C\frac{\pi^2}{L^2}\right)^{-1}\,, \tag{17}$$

and the expression (15) can be written:

$$e = \frac{C}{A^2}B_z^2\frac{\pi^2}{L^2}\,. \tag{18}$$

We have measured the curvature radius (at the axial midplane $z = 0$, and in the middle of the maximum current gradient)

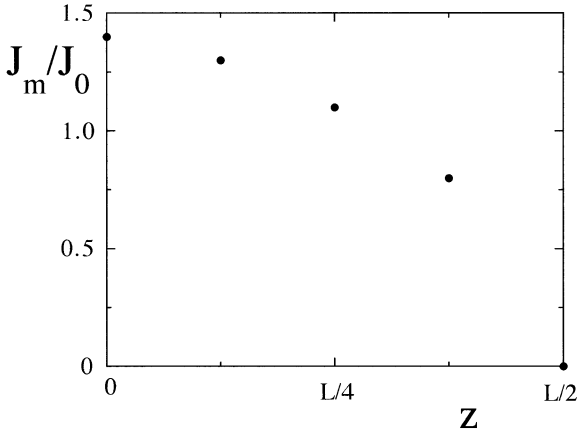

Fig. 8. The amplitude of the normalized current concentration as a function of the axial coordinate z, for the case $L/a = 4.7$

as a function of the aspect ratio of the loop in the simulations. The results are plotted in Fig. 12, and show very good agreement with the quadratic dependence given by the expression (17) if one takes $C = 0.27a$. This value of the amplitude also corresponds very well with the value of the radial displacement, as represented in Fig. 6. Then, we have measured the radial thickness e in our simulations using the following definition:

$$e = \left(\frac{1}{J_0}\frac{dJ}{dr}\right)^{-1}\,, \tag{19}$$

with J_0 the maximum value of the initial equilibrium current density. The results are plotted in Fig. 13, together with evaluations using Eq. (18), estimating $A \approx 8$ in normalized units. The physical meaning of A is given by the shear of field lines for the kinked equilibrium. We have checked that its value is of order of the above estimate, whatever the aspect ratio. Indeed, the value of A is mainly determined by the quantity of unstable magnetic energy, or equivalently by the growth rate which was taken to be approximately the same for all the simulations. Therefore, we have obtained a rather good agreement between the results of the simulations and the above simple model. The resulting current amplitudes displayed in Fig. 7 can also easily be explained by making the approximation $J_m \approx \frac{B}{e}$. It is important to note that the quadratic dependence of the radial thickness of Eq. (18) is weakened by the slow increase of B_z as a function of the aspect ratio, because of the increase of the critical twist Φ_m (see Fig. 4). Then, at the axial midplane of the loop, the scaling law of the characteristics (thickness and amplitude) of the current concentration as a function of the aspect ratio is an algebraic linear-like dependence.

As concerns the current gradients obtained at other axial planes ($z \neq 0$), we must emphasize the difficulty of obtaining a simple expression like Eq. (18) in order to describe the thickness of the current layers. However, as can be seen in Fig. 8, current gradients are less intense than in the axial midplane, and their axial variation can be described by a simple sinusoidal modulation.

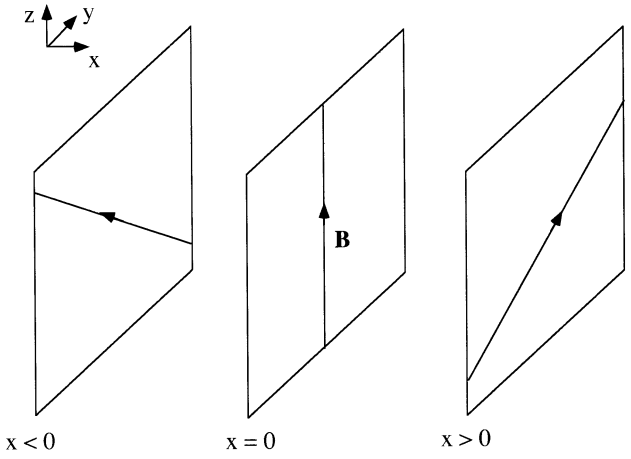

Fig. 9a. A simplified slab un-tied magnetic configuration in the vicinity of $x = 0$

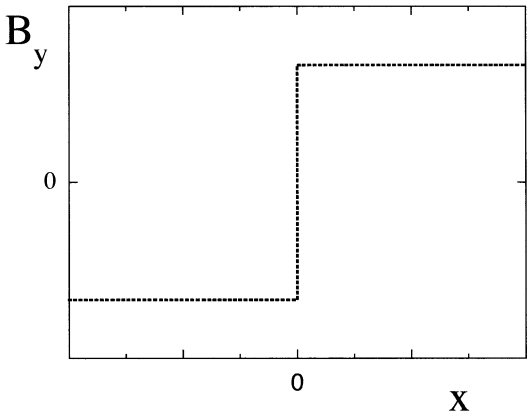

Fig. 9b. The corresponding variation of the component B_y as a function of x

4.3. Initial equilibrium profiles effects

Firstly, we have investigated the effect of the linear growth rate on the kinked equilibrium structure. When the linear growth rate is increased, the main effect is to increase the value of A, and then to lead to a smaller thickness in correlation with a higher amplitude of the current concentration. We must point out that in this study, we have chosen a given value of the linear growth rate of order $0.4\, t_a^{-1}$, as it corresponds to a characteristic time scale for the formation of current gradients sufficiently rapid compared to the typical photospheric time scale.

Secondly, we have used equilibria with different twist profiles. Particularly, we have varied the shear in the centre of the flux tube. We have observed a weak effect. The results are only changed by 20 percent when the shear is increased or reduced by a factor of two. Indeed, the effect of the initial shear is mainly to lead to a different Θ field line bending in the region considered. In the simple model considered in this study, we have neglected the Θ field line bending, assuming the bending to be dominated by the axial one, due to the line-tying effect. Therefore, this result is in agreement with our earlier assumptions.

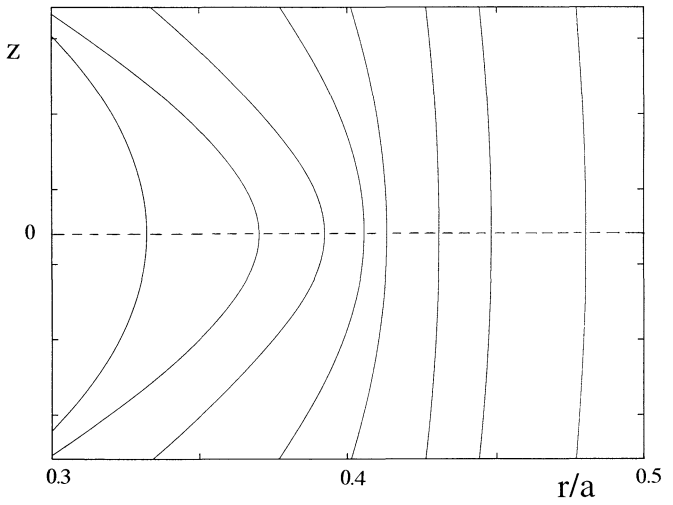

Fig. 10. The projections of different magnetic field lines in the (r,z) plane for an aspect ratio value $L/a = 4.7$, the $z = 0$ axis is represented by the hatched line

Finally, we have considered non force free initial magnetic equilibria with a gradient pressure term. The main effect is to give an additional pressure contribution for the radial force balance in Eq. (18). The simulation results have shown a weak effect when the plasma pressure is much smaller than the magnetic pressure. Hood et al. (1994) have shown that MHD instabilities with higher m mode numbers can be destabilized when pressure becomes important. However, these instabilities are beyond the scope of this paper, as we focus on low-beta $m = 1$ kink instabilities.

5. Discussion

We have presented full three dimensional MHD simulations of the non linear evolution of the ideal $m = 1$ kink mode in cylindrical line-tied coronal loops. In particular, we have provided a study of the characteristics (thickness and amplitude) of the current concentration, which is known to develop when the kink instability drives the initial magnetic configuration towards a secondary bifurcated MHD equilibrium (Baty & Heyvaerts 1996).

Firstly, we have investigated the effect of the aspect ratio of the loop. At the axial midplane of the loop, the simulation results have shown a decreasing linear-like scaling of the thickness of the current layer as a function of the aspect ratio L/a, for values of L/a in the range 2–10. The amplitude of the corresponding current density is correspondingly linearly increasing. A simple model is proposed to interpret this, with rather good agreement with the numerical results. Indeed, the line-tying effect leads to an axial field line bending which depends on the field line considered and prevents the formation of a discontinuity of the magnetic field. Then, contrary to the un-tied configuration where a genuine singular current sheet forms, the bifurcated kinked equilibrium is characterized by a force balance between

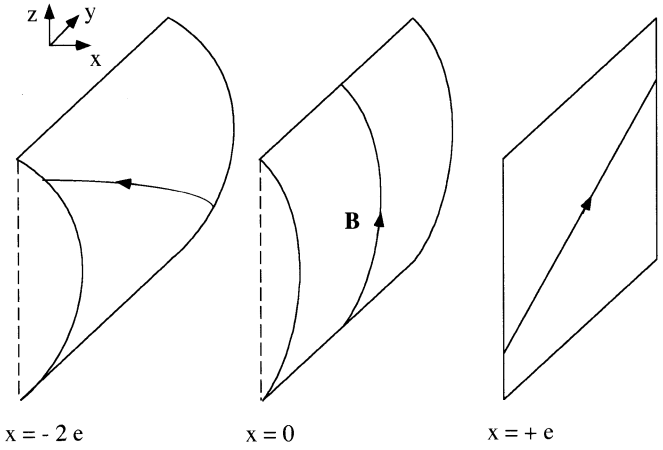

Fig. 11a. A simplified slab tied magnetic configuration in the vicinity of $x = 0$

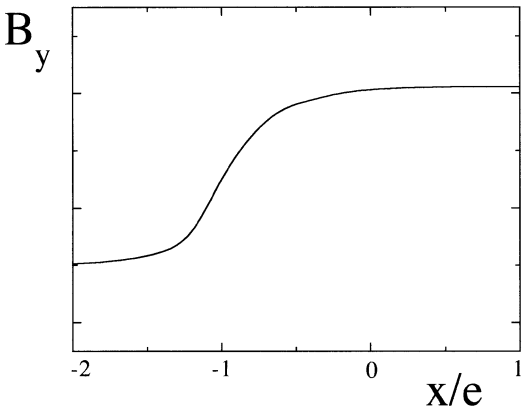

Fig. 11b. The corresponding variation of the component B_y as a function of x

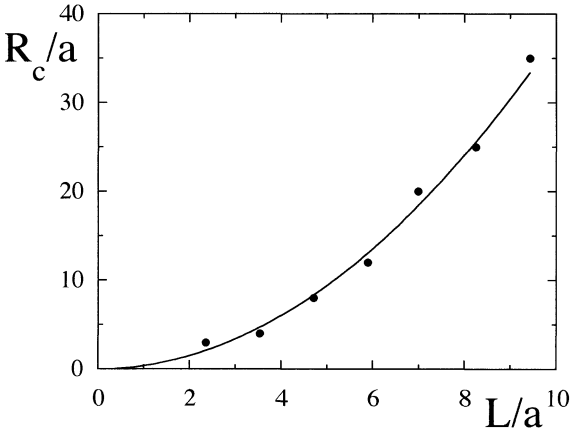

Fig. 12. The normalized curvature radius at $x = 0$ at the axial midplane $z = 0$ as a function of the aspect ratio value L/a, measured in the simulations (circles), and values obtained using Eq. (17) with $C = 0.27\,a$ (plain line)

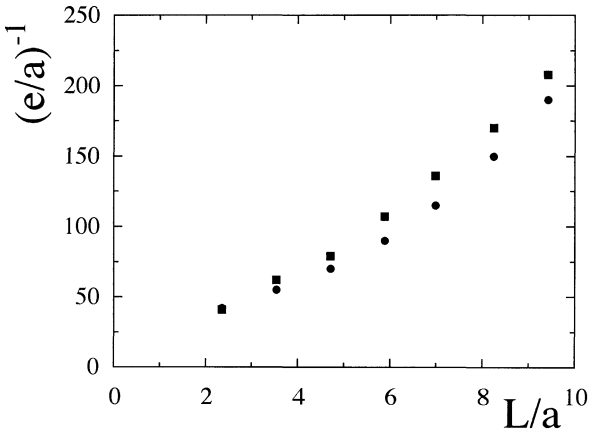

Fig. 13. The normalized thickness of the current layer at the axial midplane $z = 0$, measured in the simulations (circles), and calculated using Eq. 17 (squares) with $C = 0.27\,a$ and $A = 8$

sharp pressure gradients in the magnetic field and the curvature force due to the axial line-bending.

This effect is intimately linked to the absence of magnetic resonance in line-tied magnetic configurations and to the existence of a non-zero minimum of the Alfvén frequency (Goedbloed & Halberstaedt 1994) given by:

$$\omega_{\rm a}^2 = \frac{B_{\rm z}^2}{\rho\mu_0}\left[\frac{\pi}{L}\right]^2 . \qquad (20)$$

Indeed, one must note in Eq. (20) that the $B_{\rm z}^2\left[\frac{\pi}{L}\right]^2$ term, which is also the line-bending term arising in the expression (17), determines the thickness of the current layer.

Our result is also consistent with the recent analytical work of Longcope & Strauss (1994). These authors have found that current sheets do not form in the framework of the line-tied ideal coalescence instability. They have shown that the line-tying constraint is inconsistent with a genuine singular current sheet, but allows the formation of current layers, the thickness of which is five or six orders of magnitude smaller than the initial scale length of the equilibrium. This thickness depends exponentially on the length L between the two photospheric axial boundaries, and vanishes in the limit of infinite length L. Applying the same arguments to the line-tied ideal kink instability, they predicted a linear dependence of the thickness of current layers on the length of the loop.

We have also investigated the effect of the initial equilibrium parameters: the shear of the initial equilibrium, and the pressure gradient effect. The results indicate only weak effects on the features of the current concentration as long as the plasma pressure is dominated by the magnetic one.

Given typical values of loop parameters in active regions, it can be seen that the amount of available magnetic energy stored is sufficient to feed the observed heating flux of $10^7\,\mathrm{ergs\,cm^{-2}\,s^{-1}}$. Indeed, as the result of photospheric motions, the loop acquires an azimuthal magnetic field component B_Θ corresponding to a twist angle Φ. When Φ exceeds the critical value $\Phi_{\rm c}$, the initial configuration is rapidly driven towards a kinked configuration where $B_{\rm h} = B_\Theta(\Phi - \Phi_{\rm c})/\Phi_{\rm c}$ gives an

estimate of the magnetic field to be further dissipated. The corresponding stored magnetic energy is then:

$$W = \frac{B_{\rm h}^2}{2\mu_0}\pi a^2 L\,, \tag{21}$$

and the rate of energy transfer to the loop is given by:

$$\dot{W} = \frac{dW}{dt} \approx \frac{W}{t_{\rm p}}\,, \tag{22}$$

where $t_{\rm p}$ is the photospheric time scale necessary to induce the twist in the loop. The expression (22) leads to the average flux:

$$F = \frac{\dot{W}}{\pi a^2} = \frac{B_{\rm h}^2}{2\mu_0} L t_{\rm p}^{-1}\,. \tag{23}$$

For $B_{\rm h} = 10\,{\rm G}$, $L = 10^8\,{\rm m}$, $t_{\rm p} = 10^3\,{\rm s}$, we get $F = 4 \cdot 10^7\,{\rm ergs\,cm^{-2}\,s^{-1}}$. The problem is how to dissipate this energy quickly enough.

The subsequent conversion of the magnetic energy into heat by ohmic dissipation is a challenging aspect of the theory. Indeed, because of the smallness of classical values of the resistivity η, the resistive dissipation power ηJ^2 needed to explain the observed heating rate requires extremely large current densities $|J|$. This corresponds to a magnetic field structured on a very fine scale of order of a few meters. For typical observed loops, a scale length of about five orders of magnitude smaller than the gross features of the magnetic configuration is necessary. With our adopted parameters, the results have indicated that the gradient length scale in the kinked configuration is only two or three orders of magnitude smaller than the initial magnetic configuration one. Such magnetic features certainly lead to insufficient ohmic dissipation when classical resistivity effect is considered. However, in this work, we have restricted our computations to aspect ratio smaller than 10, mainly because of memory storage constraint of the computer. Consequently, it is necessary to explore higher values of the aspect ratio in order to investigate if the linear-like scaling law remains valid or not, or to explore whether there exists a critical length beyond which singular current sheets do form. In this study, we have also used the cylindrical geometry approximation which seems reasonable for studying the stability of loops of large aspect ratio. However, the toroidal field line bending could change the non linear force balance given by the expression (12), eventually leading to a different scaling law. These aspects remain to be investigated. Moreover, when the current density exceeds a critical value, current-driven microinstabilities (Rosner et al. 1978; Beaufumé et al. 1992) are excited leading then to an anomalous resistivity enhanced by several orders of magnitude over its classical value.

Another interesting question concerns the nature of the ohmic dissipation. It is of particular interest to determine if a reconnection mechanism takes place, as is the case in periodic magnetic configurations. It is also possible that the diffusive processes could generate some kind of MHD turbulence. We plan to study the further resistive evolution of kinked line-tied magnetic structures in future work.

Acknowledgements. The author thanks Jean Heyvaerts for fruitful discussions and careful reading of the manuscript. The numerical calculations were performed on the CRAY C98 at I.D.R.I.S., Orsay (France).

References

Aydemir A.Y., Barnes D.C., 1985, J. Comput. Phys. 59, 108
Baty H., Luciani J.F., Bussac M.N., 1991, Nucl. Fusion 31, 2055
Baty H., Luciani J.F., Bussac M.N., 1992, Nucl. Fusion 32, 1217
Baty H., Luciani J.F., Bussac M.N., 1993, Phys. Fluids B5, 1213
Baty H., Heyvaerts J., 1996, A&A 308, 935
Beaufumé P., Coppi B., Golub L., 1992, ApJ 393, 396
Califano F., Chiuderi C., Einaudi G., 1992, ApJ 390, 560
Chiuderi C., Einaudi G., Ma S.S., Van Hoven G., 1980, J. Plasma Phys. 24, 1
Craig I.J. D., Mc Clymont A.N., Sneyd A.D., 1988, ApJ 335, 441
Craig I.J. D., Sneyd A.D., 1990, ApJ 357, 653
Einaudi G., Van Hoven G., 1983, Solar Phys. 88, 163
Einaudi G, Mok Y., 1987, ApJ 319, 520
Goedbloed J.P., Halberstadt G., 1994, A&A 286, 275
Halberstadt G., Goedbloed J.P., 1993, A&A 280, 647
Halberstadt G., Goedbloed J.P., 1995, A&A 301, 577
Heyvaerts J., 1992, in: Damé L., Guyenne T.D. (eds), ESA Aimuris Workshop, Solar Physics and Astrophysics and Interferometric Resolution SP 344, Paris, France, p.69
Heyvaerts J., Priest E.R., 1984, A&A 137, 63
Heyvaerts J., Priest E.R., 1992, ApJ 390, 297
Hollweg J.V., 1987, ApJ 312, 880
Hood A.W., Priest E.R., 1979, Solar Phys. 64, 303
Hood A.W., De Bruuyne P., Van Der Linden R.A.M., Gooseens M., 1994, Solar Phys 150, 99
Ionson J.A., 1978, ApJ 226, 65
Lerbinger K., Luciani J.F., 1991, J. Comput. Phys. 97, 444
Longbottom A.W., Hood A.W., Rickard G.J., 1996, Plasma Phys. Control. Fusion 38, 193
Longcope D.W., Strauss H.R., 1994, ApJ 437, 851
Mikic Z., Schnack D.D., 1990, ApJ 361, 690
Mok Y., Van Hoven G., 1982, Phys. Fluids 25, 636
Otani N.F., Strauss H.R., 1988, ApJ 325, 468
Park W., Monticello D.A., White R.B., Jardin S.C., 1980, Nucl. Fusion 20, 1181
Parker E.N., 1983, ApJ 264, 642
Poedts S., Belien A.J.C., Goedbloed J.P., 1994, Solar Phys. 151, 271
Raadu M.A., 1972, Solar Phys. 22, 425
Rosenbluth M.N., Dagazian R.Y., Rutherford P.H., 1973, Phys. Fluids 16, 1894
Rosner R., Golub L., Coppi B., Vaiana G.S., 1978, ApJ 222, 317
Strauss H.R., Otani N.F., 1988, ApJ 326, 418
Van Ballegooijen A.A., 1986, ApJ 311, 1001
Velli M., Einaudi G., Hood A.W., 1990 (a), ApJ 350, 428
Velli M., Einaudi G., Hood A.W., 1990 (b), ApJ 350, 419
Waelbroeck F.L., 1989, Phys. Fluids B1, 2372